VOLUME 35 | SUPPLEMENT 2 | MARCH 2022

MODERN PATHOLOGY

ABSTRACTS (508–521)

GENERAL SURGICAL PATHOLOGY

2022

USCAP 111TH ANNUAL MEETING

REAL INTELLIGENCE

MARCH 19–24, 2022 LOS ANGELES, CALIFORNIA

Published by
SPRINGER NATURE
www.ModernPathology.org

USCAP Creating a Better Pathologist
AN OFFICIAL JOURNAL OF THE UNITED STATES AND CANADIAN ACADEMY OF PATHOLOGY

EDUCATION COMMITTEE

Rhonda K. Yantiss
Chair

Kristin C. Jensen
Chair, CME Subcommittee

Laura C. Collins
Chair, Interactive Microscopy Subcommittee

Yuri Fedoriw
Short Course Coordinator

Ilan Weinreb
Chair, Subcommittee for Unique Live Course Offerings

Carla L. Ellis
Chair, DEI Subcommittee

Adebowale J. Adeniran
Kimberly H. Allison
Sarah M. Dry
William C. Faquin
Karen J. Fritchie
Jennifer B. Gordetsky
Levon Katsakhyan, Pathologist-in-Training
Melinda J. Lerwill
M. Beatriz S. Lopes
Julia R. Naso, Pathologist-in-Training
Liron Pantanowitz
Carlos Parra-Herran
Rajiv M. Patel
Charles "Matt" Quick
David F. Schaeffer
Lynette M. Sholl
Olga K. Weinberg
Maria Westerhoff

ABSTRACT REVIEW BOARD

Benjamin Adam
Oyedele Adeyi
Mariam Priya Alexander
Daniela Allende
Catalina Amador
Vijayalakshmi Ananthanarayanan
Tatjana Antic
Manju Aron
Roberto Barrios
Gregory R. Bean
Govind Bhagat
Luis Zabala Blanco
Michael Bonert
Alain C. Borczuk
Tamar C. Brandler
Eric Jason Burks
Kelly J. Butnor
Sarah M. Calkins
Weibiao Cao
Wenqing (Wendy) Cao
Barbara Ann Centeno
Joanna SY Chan
Kung-Chao Chang
Hao Chen
Wei Chen
Yunn-Yi Chen
Sarah Chiang
Soo-Jin Cho
Shefali Chopra
Nicole A. Cipriani
Cecilia Clement
Claudiu Cotta
Jennifer A. Cotter
Sonika M. Dahiya
Elizabeth G. Demicco
Katie Dennis
Jasreman Dhillon
Anand S. Dighe
Bojana Djordjevic
Michelle R. Downes
Charles G. Eberhart
Andrew G. Evans
Fang Fan
Julie C. Fanburg-Smith
Gelareh Farshid
Michael Feely
Susan A. Fineberg
Dennis J. Firchau
Gregory A. Fishbein
Agnes B. Fogo
Andrew L. Folpe
Danielle Fortuna
Billie Fyfe-Kirschner
Zeina Ghorab
Giovanna A. Giannico
Anthony J. Gill
Tamar A. Giorgadze
Alessio Giubellino
Carolyn Glass
Carmen R. Gomez-Fernandez
Shunyou Gong
Purva Gopal
Abha Goyal
Christopher C. Griffith
Ian S. Hagemann
Gillian Leigh Hale
Suntrea TG Hammer
Malini Harigopal
Kammi J. Henriksen
Jonas J. Heymann
Carlo Vincent Hojilla
Aaron R. Huber
Jabed Iqbal
Shilpa Jain
Vickie Y. Jo
Ivy John
Dan Jones
Ridas Juskevicius
Meghan E. Kapp
Nora Katabi
Francesca Khani
Joseph D. Khoury
Benjamin Kipp
Veronica E. Klepeis
Christian A. Kunder
Stefano La Rosa
Stephen M. Lagana
Keith K. Lai
Goo Lee
Michael Lee
Vasiliki Leventaki
Madelyn Lew
Faqian Li
Ying Li
Chieh-Yu Lin
Mikhail Lisovsky
Lesley C. Lomo
Fang-I Lu
aDeqin Ma
Varsha Manucha
Rachel Angelica Mariani
Brock Aaron Martin
David S. McClintock
Anne M. Mills
Richard N. Mitchell
Hiroshi Miyamoto
Kristen E. Muller
Priya Nagarajan
Navneet Narula
Michiya Nishino
Maura O'Neil
Scott Roland Owens
Burcin Pehlivanoglu
Deniz Peker Barclift
Avani Anil Pendse
Andre Pinto
Susan Prendeville
Carlos N. Prieto Granada
Peter Pytel
Stephen S. Raab
Emilian V. Racila
Stanley J. Radio
Santiago Ramon Y Cajal
Kaaren K Reichard
Jordan P. Reynolds
Lisa M. Rooper
Andrew Eric Rosenberg
Ozlen Saglam
Ankur R. Sangoi
Kurt B. Schaberg
Qiuying (Judy) Shi
Wonwoo Shon
Pratibha S. Shukla
Gabriel Sica
Alexa Siddon
Anthony Sisk
Kalliopi P. Siziopikou
Stephanie Lynn Skala
Maxwell L. Smith
Isaac H. Solomon
Wei Song
Simona Stolnicu
Adrian Suarez
Paul E. Swanson
Benjamin Jack Swanson
Sara Szabo
Gary H. Tozbikian
Gulisa Turashvili
Andrew T. Turk
Efsevia Vakiani
Paul VanderLaan
Hanlin L. Wang
Stephen C. Ward
Kevin M. Waters
Jaclyn C. Watkins
Shi Wei
Hannah Y. Wen
Kwun Wah Wen
Kristy Wolniak
Deyin Xing
Ya Xu
Shaofeng N. Yan
Zhaohai Yang
Yunshin Albert Yeh
Huina Zhang
Xuchen Zhang
Bihong Zhao
Lei Zhao

To cite abstracts in this publication, please use the following format: **Author A, Author B, Author C, et al. Abstract title (abs#). In "File Title."** ***Modern Pathology*** **2022; 35 (suppl 2): page#**

508 Extragonadal Germ Cell Tumors: A Comprehensive Study with Emphasis on Morphological Features, Clinical Outcomes and Associated Secondary Malignancies

Eman Abdulfatah[1], Noah Brown[2], Zachery Reichert[2], Tao Huang[2], Sandra Camelo-Piragua[2], Amer Heider[2], Khaled Hafez[2], Todd Morgan[2], Matthew Davenport[2], Ulka Vaishampayan[2], Stephanie Skala[2], Daniel Spratt[3], Jeffrey Montgomery[2], Liron Pantanowitz[2], Arul Chinnaiyan[2], Lina Shao[2], Rohit Mehra[2]

[1]Michigan Medicine, University of Michigan, Ann Arbor, MI, [2]University of Michigan, Ann Arbor, MI, [3]UH Cleveland Medical Center, Cleveland, OH

Disclosures: Eman Abdulfatah: None; Noah Brown: None; Zachery Reichert: None; Tao Huang: None; Sandra Camelo-Piragua: None; Amer Heider: None; Khaled Hafez: None; Todd Morgan: None; Matthew Davenport: None; Ulka Vaishampayan: None; Stephanie Skala: None; Daniel Spratt: None; Jeffrey Montgomery: None; Liron Pantanowitz: None; Arul Chinnaiyan: None; Lina Shao: None; Rohit Mehra: None

Background: Extragonadal germ cell tumors (EGCT) are rare, representing <5% of all germ cell tumors (GCTs). They demonstrate a variety of histologic subtypes, anatomic distributions, and clinical settings. Whilst EGCT share morphological and immunohistochemical features with their gonadal counterparts, they tend to be more aggressive and are frequently associated with secondary somatic malignancies. Providing an accurate diagnosis is challenging but important for establishing prognosis and directing therapy. Here in, we report a series of EGCT with focus on their pathology and clinical outcomes.

Design: EGCT patients diagnosed from 2001-2020 were identified. Only patients with absence of gonadal masses on physical examination and radiology were included. H&E slides were reviewed by 2 GU pathologists to evaluate morphologic features and IHC (SALL4,CD117,PLAP,OCT4,CD30,AFP,Glypican-3 and HCG). Clinical, radiological, treatment and follow-up data were recorded.

Results: 77 EGCT patients were included. Median age was 18 years (range 1 day-68 years). The cohort consisted of 71% males and 29% females. One patient had Klinefelter syndrome. Median tumor size was 6 cm (range 1-21.5 cm). Anterior mediastinum was the most common anatomic site (38%), followed by central nervous system (CNS)(34%), retroperitoneum (11%), sacrococcygeal region (11%) and neck (6%). Histologically, pure GCTs were more common than mixed GCTs (71%vs.29%); Seminoma was the most common pure GCT encountered. Amongst mixed GCTs, the most common combination was yolk sac tumor(YST), mature and immature teratoma. In anterior mediastinum, pure or mixed YST was most common. Seminoma was most common in CNS. Teratoma (mature and immature) was most common in sacrococcygeal region. Endodermal sinus pattern was the most common growth patten seen in YST. Solid and glandular patterns were most frequent in embryonal carcinomas. IHC expression for all markers was similar to testicular GCTS. Somatic-type malignancies (STM) were identified in 6% of tumors with rhabdomyosarcoma being most common(n=2/5), followed by MPNST(n=1/5), undifferentiated round cell sarcoma(n=1/5) and adenocarcinoma(n=1/5). One patient had concurrent acute myeloid leukemia with megakaryoblastic differentiation and 1 patient developed myelodysplastic syndrome a year later. Both were diagnosed with anterior mediastinal EGCT. Patients underwent either chemotherapy and radiation therapy (RT)(n=23),resection only(n=17), resection and chemotherapy(n=12), chemotherapy only(n=3),resection, chemotherapy and RT(n=1) and unknown(n=21). Disease progression (metastasis and/or recurrence) was documented in 8 patients, all of whom died from their relapse. Two patients who died of disease had STM.

Conclusions: Our results demonstrate that EGCT share similar histologic features but diverse clinical outcomes compared to their gonadal counterparts. The majority of these patients undergo chemotherapy and RT. These data corroborate that STM are frequently encountered and that their presence portends a poorer prognosis.

509 Multicenter Harmonization Study for pan-Trk Immunohistochemistry

Julien Adam[1], Nolwenn Le Stang[2], Arnaud Uguen[3], Marie-Pierre Chenard, Sylvie Lantuejoul[2], Aurelie Maran-Gonzalez[4], Yves Robin, Philippe Rochaix[5], Jean-Christophe Sabourin[6], Isabelle Soubeyran[7], Nathalie Sturm[8], Magali Svrcek[9], Anne Vincent-Salomon[10], Nina Radosevic-Robin[11], Frederique Penault-Llorca[11]
[1]Hôpital St Joseph, Paris, France, [2]Centre Léon Bérard, Lyon, France, [3]Cavale Blanche - Brest University Hospital, Brest, France, [4]ICM (Institut du Cancer de Montpellier), Nantes, France, [5]Institut Claudius Regaud, IUCTO, [6]Rouen University Hospital, Rouen, France, [7]Institut Bergonié, [8]CHU de Grenoble, Grenoble, France, [9]Sorbonne University, Assistance Publique Hôpitaux de Paris, Paris, France, [10]Institut Curie, Paris, France, [11]Centre Jean Perrin, Clermont-Ferrand, France

Disclosures: Julien Adam: *Grant or Research Support*, Bayer; Nolwenn Le Stang: None; Arnaud Uguen: None; Marie-Pierre Chenard: None; Sylvie Lantuejoul: None; Aurelie Maran-Gonzalez: None; Yves Robin: None; Philippe Rochaix: None; Jean-Christophe Sabourin: *Consultant*, AstraZeneca, Servier, BMS, MSD, AMGEN; Isabelle Soubeyran: None; Nathalie Sturm: None; Magali Svrcek: None; Anne Vincent-Salomon: *Advisory Board Member*, Ibex; Nina Radosevic-Robin: None; Frederique Penault-Llorca: None

Background: Pan-Trk immunohistochemistry (IHC) has been described as a screening test for the detection of *NTRK* fusions in a broad spectrum of tumor types. However, pan-Trk testing in the clinical setting may be limited by many factors, including analytical parameters such as clones, platforms and protocols used. This study aimed at harmonizing pan-Trk testing using various clones and IHC platforms and evaluate the level of analytical variability across pathology laboratories.

Design: IHC laboratory-developed tests (LDT) were developed using pan-Trk clones EPR17341 (Abcam) and A7H6R (Cell Signaling Technology) for Ventana/Roche, Agilent and Leica platforms. TMA including 9 cases with *NTRK* fusions were sent to pathology laboratories in order to perform stainings on Ventana/Roche (10 centers), Agilent (4 centers) and Leica (3 centers) platforms. A ready-to-use pan-Trk IVD assay (Ventana/Roche) was also performed in 3 centers. All stainings were centrally and blindly reviewed for the percentage of stained tumor cells.

Results: LDT protocols with clone EPR17341 were able to detect pan-Trk protein expression in all cases, whereas lower rates of positivity were observed with clone A7H6R. Moderate to strong variability in the rate of positive cases was observed for both antibodies in the three types of IHC platforms for the three positivity cut-points evaluated (≥1%, ≥10% and ≥50%). The rate of false negative cases was lower when pan-Trk staining was assessed with the lowest positivity threshold (≥1% of stained tumor cells).

Conclusions: Most evaluated pan-Trk IHC LDT were able to detect *NTRK*-fusion protein expression, however a significant analytical variability was observed between antibodies, platforms and centers. The use of low positivity threshold (≥1%) may partly counterbalance this analytical variability.

510 Immunohistochemical Expression of Carbonic Anhydrase IX, Glucose Transporter 1 and Paired Box 8 in von Hippel Lindau Disease-Related Lesions

Kyriakos Chatzopoulos[1], Marie-Christine Aubry[1], Sounak Gupta[1]
[1]Mayo Clinic, Rochester, MN

Disclosures: Kyriakos Chatzopoulos: None; Marie-Christine Aubry: None; Sounak Gupta: None

Background: von Hippel Lindau (VHL) disease is a genetic syndrome resulting from pathogenic alterations of the *VHL* tumor suppression gene, manifesting with cysts and tumors in multiple organ systems. VHL protein (pVHL) is a known downregulator of hypoxia inducible factor-1a (HIF1a). Loss of function of pVHL is associated with upregulation of the HIF1a pathway including carbonic anhydrase IX (CAIX), and glucose transporter-1 (GLUT1). Paired Box 8 (PAX8) is an important transcription factor-regulator of mesonephric development. We investigated the role of immunohistochemistry in assessment of CAIX, GLUT1 and PAX8 expression in VHL-related lesions.

Design: Clinicopathologic information and archival surgical and autopsy pathology material from 5 patients with VHL disease, treated between 2004-2021 was retrospectively reviewed and evaluated for expression of: CAIX (clone EP161, Cell Marque, Rocklin, CA); GLUT1 (polyclonal antibody, Cell Marque, Rocklin, CA); and PAX8 (clone SP348 N-terminal, Abcam, Cambridge, MA).

Results: The clinicopathologic features of the 5 patients with VHL disease, as well as the immunophenotype of their VHL-related lesions, are presented in Table 1. CAIX and GLUT1 was expressed in all VHL-related lesions and exhibited diffuse positivity and

membranous localization (15/15 lesions, 100%; 5/5 patients), including microscopically identified pulmonary microcysts. PAX8 was expressed only in renal and epididymal lesions.

Table 1: Clinicopathologic characteristics of patients with von Hippel Lindau disease and immunophenotype of related lesions

Patient	Age	Sex	*VHL* mutation status	Tumor type	CAIX	GLUT1	PAX8
1	19	Female	c.488T>C	Hemangioblastoma	Positive	Positive	Negative
				Pulmonary microcysts	Positive	Positive	Negative
2	40	Male	c.620T>C	Epididymal papillary cystadenoma	Positive	Positive	Positive
				Hemangioblastoma	Positive	Positive	Negative
				Cystic clear cell renal cell carcinoma	Positive	Positive	Positive
				Pancreatic neuroendocrine tumor	Positive	Positive	Negative
3	42	Female	c.292T>C	Bilateral pheochromocytoma	Positive	Positive	Negative
				Hemangioblastoma	Positive	Positive	Negative
4	51	Female	Pathogenic alteration, per clinical notes	Hemangioblastoma	Positive	Positive	Negative
				Bilateral renal cysts	Positive	Positive	Positive
				Bilateral clear cell renal cell carcinoma	Positive	Positive	Positive
				Pancreatic serous cystadenoma	Positive	Positive	Negative
				Bilateral pulmonary microcysts	Positive	Positive	Negative
5	54	Male	Possible somatic mosaic	Endolymphatic sac tumor	Positive	Positive	Negative
				Bilateral renal cysts	Positive	Positive	Positive

Conclusions: CAIX and GLUT1 are consistently overexpressed in VHL-related lesions, reflecting upregulation of the HIF1a pathway, secondary to defects in pVHL. PAX8 is only expressed in genitourinary lesions, mirroring organ-specific differentiation. A combination of CA-IX and GLUT1 immunostains is useful in screening lesions of patients with VHL-spectrum manifestations, which may be targeted by recently FDA approved HIF-2a inhibitors.

511 Tumor Stroma Originates from Bone Marrow-Derived Mesenchymal Cells: An In Situ Analysis of Cancer Samples from Patients Post Allogeneic Sex-Mismatched Bone Marrow Transplant

Fatemeh Derakhshan[1], Yanyun Li[1], Ozge Birsoy[1], Higinio Dopeso[1], Fresia Pareja[1], Ryan Ptashkin[1], Tony El Jabbour[2], Hannah Wen[1], Edi Brogi[1], Britta Weigelt[1], Yanming Zhang[1], Travis Hollmann[1], Jorge Reis-Filho[1], Diana Mandelker[1]
[1]Memorial Sloan Kettering Cancer Center, New York, NY, [2]Mount Sinai Hospital, New York, NY

Disclosures: Fatemeh Derakhshan: None; Yanyun Li: None; Ozge Birsoy: None; Higinio Dopeso: None; Fresia Pareja: None; Ryan Ptashkin: None; Tony El Jabbour: None; Hannah Wen: *Consultant*, AstraZeneca; *Consultant*, Merck; Edi Brogi: None; Britta Weigelt: *Advisory Board Member*, Repare Therapeutics; Yanming Zhang: None; Travis Hollmann: None; Jorge Reis-Filho: *Consultant*, Paige, Repare Therapeutics; *Advisory Board Member*, Roche Tissue Diagnostic, Grupo Oncoclinicas/ Goldman Sachs; Diana Mandelker: None

Background: Bone marrow-derived stem cells participate in tissue repair after injury. The contribution of bone marrow derived stem cells to solid tumors and their microenvironment (TME) has not yet been elucidated. Here, we sought to define whether the tumor cells or the tumor associated TME may be donor derived.

Design: From a pan-cancer cohort of tumors subject to tumor/normal sequencing using an FDA-cleared multi-gene sequencing assay, 20 patients who developed cancers after myeloablation and allogeneic bone marrow transplant (aBMT), were identified based on the presence of donor DNA in their tumor specimens. Eight of these patients had sex-mismatched aBMT and combined immunolabeling (CD45, vimentin, and tumor-specific markers) and fluorescence *in situ* hybridization with X and Y probes were performed, to determine the origin of the donor-derived DNA in the tumor specimens.

Results: The 8 solid organ cancers diagnosed after sex-mismatched allogeneic aBMT included 2 prostate adenocarcinoma, 2 hepatocellular carcinoma (HCC), 1 skin squamous cell carcinoma, 1 pancreatic adenocarcinoma, 1 meningioma and 1 high-grade serous ovarian cancer (HGSC). The solid tumors developed after a mean of 6.7 (1–18) years from the aBMT and demonstrated sexual chimerism, 4 of which were XX donor and 4 were XY donor. Multiplexed analysis with CD45 (pan-immune cell marker), vimentin (mesenchymal stromal marker), and cancer-specific markers (PAX8 for HGSC, CAM5.2 for HCC, S100 for meningioma) of the cancer samples from the four aBMT patients with XY donor specimens demonstrated that a subset of the CD45-positive inflammatory cells and vimentin-positive mesenchymal stroma cells were XY-donor-derived, whereas the malignant cells were of-XX-host origin. The vimentin-positive XY-donor-derived cells were part of tumor stroma only and could not be detected in the stroma away from the tumor.

Conclusions: Bone marrow-derived mesenchymal cells contribute to the TME, whereas normal surrounding mesenchymal tissues are predominantly composed of host-derived mesenchymal cells. Our findings support the contention that a large proportion of the TME stems from the bone marrow rather than pre-existent, tissue resident mesenchymal and inflammatory cells.

512 Condyloma Acuminatum can Harbor Co-Existing High-Grade Squamous Intraepithelial Lesion (HSIL) or Invasive Squamous Cell Carcinoma and Show Mixed p16 Immunostaining

Chien-Kuang Cornelia Ding[1], Peyman Samghabadi[2], Cynthia Gasper[2]
[1]University of California, San Francisco, San Francisco, CA, [2]UCSF Pathology, San Francisco, CA

Disclosures: Chien-Kuang Cornelia Ding: None; Peyman Samghabadi: None; Cynthia Gasper: None

Background: Condyloma acuminatum are common squamous papillary lesions caused by human papilloma virus (HPV). Conventional wisdom is that over 90% of condylomas are caused by low-risk HPV types and are considered benign. However, up to 50% are reported to be co-infected with high-risk HPV. High-risk HPV can cause high-grade squamous intraepithelial lesion (HSIL), and compared to condylomas, HSIL carries a significant risk of progression to invasive squamous cell carcinoma (SCC). Prior small case series have described mixed condylomas with HSIL or SCC. However, there remain few detailed clinicopathologic studies of these mixed lesions.

Design: Immunostaining for p16 as a surrogate marker for high-risk HPV were performed on whole slide sections of 30 condylomas with concurrent HSIL, 19 condylomas with concurrent invasive SCC, 12 atypical condylomas, and 11 condylomas. Atypical condylomas were defined as condylomas with either expansion of basaloid cells into the upper thirds of the epithelium or severe nuclear atypia without other features diagnostic of HSIL. Strong and diffuse nuclear and cytoplasmic block positive staining was considered p16 positive.

Results: Immunostaining for p16 was observed in 50% of atypical condylomas. In condylomas with concurrent HSIL, immunostaining for p16 was observed in 50% of the condyloma area and 100% of the HSIL area. In condylomas with concurrent SCC, immunostaining for p16 was observed in 60% of the condyloma area and 90% of the SCC area. Most subjects with concurrent condyloma and HSIL/ or invasive SCC were male and most were reported in the anal or perianal region. Only 70% of concurrent condyloma-HSIL and 60% of concurrent condyloma-invasive SCC were from immunocompromised subjects.

Table 1: Clinicopathologic Features

	Condyloma	**Atypical condyloma**	**HSIL in condyloma**	**SCC in condyloma**
Subjects	11	12	30	19
Age, average (range)	42 (19-70)	42 (25-78)	39 (24-78)	49 (38-70)
Male sex	54%	75%	77%	90%
Immunocompromised	54%	60%	70%	60%
Location				
Anal	45%	65%	60%	80%
Perianal	0%	10%	20%	10%
Vulva	35%	0%	5%	10%
Cervix	10%	25%	10%	0%
Penis	10%	0%	5%	0%
Persistence/recurrence	10%	50%	50%	30#
Average size mm (range)	20 (3-90)	14 (1-37)	22 (3-70)	25 (3-50)
Condyloma area				
Atypical mitosis	0%	25%	5%	10%
Positive p16 IHC	0%	50%	50%	60%
HSIL area				

Amount HSIL, average (range)	NA	NA	30% (5-80%)	36% (5-70%)
Atypical mitosis	NA	NA	40%	50%
Positive p16 IHC	NA	NA	100%	90%
SCC area				
Superficially invasive	NA	NA	NA	50%
Depth, average, mm (range)	NA	NA	NA	2.4 (0.1-9)
Size of invasion, mm (range)	NA	NA	NA	3.8 (0.1-25)
Well-differentiated	NA	NA	NA	60%
Positive p16 IHC	NA	NA	NA	90%
Atypical mitosis	NA	NA	NA	50%
Marked nuclear atypia	0%	10%	30%	70%
HSIL, high-grade squamous intraepithelial lesion; SCC, squamous cell carcinoma; IHC, immunohistochemistry; NA, not applicable				

Conclusions: Condylomas that harbor foci of HSIL or invasive SCC and atypical condylomas all show p16 immunostaining in morphologic areas of condyloma and HSIL or SCC suggesting involvement by high-risk HPV. Previous studies of concurrent condylomas with HSIL or SCC were seen entirely in immunocompromised subjects leading to the recommendation of careful pathologic examination of condylomas in these patients. Here we show that mixed lesions can occur in immunocompetent subjects as well. This indicates that careful pathologic examination of condylomas should be performed in all patients. Another key observation was an increased number of mixed lesions in the anal and perianal region which is likely due to the increased incidence of high-risk HPV in anal condylomas.

513 Primary Indolent Lymphomas in the Genitourinary Tract and the Significance of Workup in Suspicious Atypical B-Cell Infiltrates

Mariam Ghafoor[1], Namra Ajmal[1], Elizaveta Flerova[1], Nneamaka Nwaoduah[1], Peter Mccue[2], Li Li[1]
[1]Thomas Jefferson University Hospital, Philadelphia, PA, [2]Thomas Jefferson University, Philadelphia, PA

Disclosures: Mariam Ghafoor: None; Namra Ajmal: None; Elizaveta Flerova: None; Nneamaka Nwaoduah: None; Peter Mccue: None; Li Li: None

Background: Genitourinary (GU) tract lymphomas are a rare entity, comprising <5% of extra-nodal lymphomas, mostly involving kidneys and testes. The information about primary lymphoma as initial presentation involving prostate, bladder, and ureter is more limited. Our study provides the prevalence of primary subtypes of lymphoma in the GU organs and the significance of hematopathologic workup of the cases to identify lymphoma to guide treatment.

Design: A retrospective study of the cases with the diagnosis of lymphomas in the GU organs (kidney, prostate, bladder, testis, and ureter) between 1/1/2011 and 9/16/2021 at our institution was performed. The study only included lymphoid neoplasms.

Results: A total of 30 cases of lymphoma in the GU organs were found. 22 cases were primary lymphomas including diffuse large B-cell lymphoma (DLBCL), chronic lymphocytic leukemia/small lymphocytic lymphoma (CLL/SLL), extra-nodal marginal zone lymphoma (MZL), mantle cell lymphoma (MCL), follicular lymphoma (FL), and monoclonal B-cell lymphoproliferative disease. The most common lymphoma was DLBCL (40%) followed by CLL/SLL (23%). The most common involved organ was kidney (50%), followed by bladder (17%), testes (17%), and prostate (13%). Most prostate lymphomas are primary (3/4 cases), while 80% of bladder cases were secondary. Many lymphoma cases were incidental findings especially in the small biopsies/chips, including 1 case of MCL that was identified in the prostate chips (Image 1, A), 1 case of extra-nodal MZL involving both prostate chips and bladder biopsy; and 1 case with nephrotic range proteinuria that showed proliferative glomerulonephritis with monoclonal immunoglobulin deposits (PGNMID, IgM kappa) due to CLL/SLL involving kidney (Table 1, Image 1, B-D).

Site	Diagnosis	Primary/ Secondary	Organ involvement in secondary Cases	Mean Age at Diagnosis (years)	Gender (M: F)
Kidney (n=15)	DLBCL (n=6)	Primary (n=3) Secondary (n=3)	Intra-abdominal and inguinal LNs, jejunal mass	73.7 67.3	2:1 2:1
	CLL/SLL (n=4)	Primary (n=1) Secondary (n=3)	BM, blood, LN	71 73	1:0 3:1
	Follicular lymphoma (n=1)	Secondary (n=1)	LNs, right parotid mass	59	0:1
	Marginal zone lymphoma (n=1)	Secondary (n=1)	Orbital and systemic involvement	67	1:0
	DLBCL/Burkitt (gray zone) lymphoma(n=1)	Secondary (n=1)	BM and pleural fluid	70	0:1
	B-cell NHL (n=1)	Primary (n=1)		80	1:0
Bladder (n=5)	Marginal zone lymphoma (n=1)	Primary (n=1)		79	1:0
	CLLSLL (n=2)	Secondary (n=2)	LN	73	2:0
	DLBCL (n=1)	Secondary (n=1)	Involving cecum, liver and periumbilical area	57	1:0
	Monoclonal BLPD (n=1)	Secondary (n=1)	History of BLPD	81	1:0
Testis (n=5)	DLBCL (n=5)	Primary (n=5)		63.4	5:0
Prostate (n=4)	CLL/SLL (n=1)	Primary (n=1)		72	1:0
	Marginal zone lymphoma (n=1)	Primary (n=1)		79	1:0
	Low-grade BLPD (n=1)	Primary (n=1)		60	1:0
	Mantle cell lymphoma (n=1)	Secondary (n=1)	Salivary gland	82	1:0
Ureter (n=1)	Follicular lymphoma (n=1)	Secondary (n=1)	Retroperitoneal, peri-ureteral mass	84	1:0

Table 1. BLPD: B-cell lymphoproliferative disease; BM: Bone Marrow; CLL/SLL: Chronic Lymphocytic Leukemia/Small Lymphocytic Lymphoma; DLBCL: Diffuse Large B-Cell Lymphoma; NHL: Non-Hodgkin lymphoma; FL: Follicular Lymphoma; LN: Lymph node; M: Male, F: Female

Figure 1 - 513

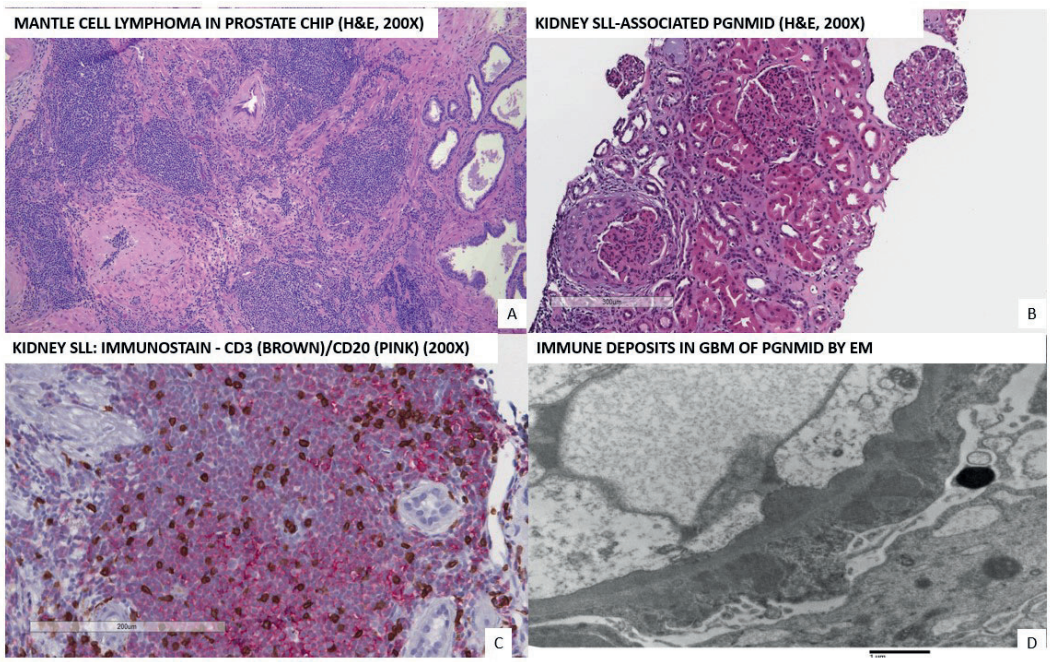

Conclusions: Lymphoma involving the GU organs is rare, and lymphocytic infiltrates in the GU organs are rarely worked up. Our study emphasizes the variety of lymphomas that can be seen in the GU tract. The recognition of the subtypes of lymphoma with

hematopathologic workup in the GU organs is critical for early diagnosis and treatment options, especially for indolent and/or aggressive lymphomas like MCL.

514 Specificity of Immunohistochemistry for Mycobacteria Using the Biocare Rabbit Polyclonal Antibody

Lauren Kroll-Wheeler[1], Steven Hrycaj[1], May Chan[1], Jerome Cheng[1], Laura Lamps[1]
[1]*University of Michigan, Ann Arbor, MI*

Disclosures: Lauren Kroll-Wheeler: None; Steven Hrycaj: None; May Chan: None; Jerome Cheng: None; Laura Lamps: None

Background: Tissue biopsy with special stains for acid-fast bacilli (AFB) is often the most efficient way to establish a diagnosis of mycobacterial infection. However, organisms are often sparse or focal, and evaluation may be limited by over-decolorization and other technical limitations. Recent publications have featured an immunohistochemical antibody as a sensitive tool for detecting *M. tuberculosis* and non-tubercular mycobacteria. Studies of its specificity, however, have been limited to cases clinically or microscopically suspected of mycobacterial infection, and its performance with a wide variety of non-mycobacterial infections has not been investigated

Design: Thirty-six cases representing a variety of pathogens, tissue types, and inflammatory responses were included. The cases were reviewed by three pathologists, along with any pertinent special stains and culture or molecular results, and then stained with the Biocare rabbit polyclonal antimycobacterial antibody (Biocare Medical, Pacheco, CA) for detection of mycobacteria.

Results: All 3 cases of mycobacterial infection stained positively with mycobacterial immunohistochemistry (mIHC) (Figure 1). *Pseudomonas* (3/3 cases), *Nocardia* (1/1), and *Actinomyces* (1/1) were similarly positive for mIHC. Another 9 of 10 mixed or nonspecific bacterial infections also stained positively, including bacterial colonization of the upper aerodigestive tract, bullous impetigo, and mixed deep tissue infections with enterococcus and MRSA. *Blastomyces* (1/1), chromoblastomycosis (1/1), and *Coccidioides* (1/1) had capsules that stained positive for mIHC. One case of leishmaniasis was also immunoreactive (Figure 2). Other bacterial and fungal organisms tested were negative for mIHC (Table 1).

Table 1. Cases stained for Biocare rabbit polyclonal antimycobacterial antibody with pertinent clinical information and special stains results. *Special stains included Twort's Gram stain (Twort), Gomori Methenamine Silver stain (GMS), Fite's Acid Fast stain (Fite), Ziehl-Neelsen acid fast stain (ZN), and immunohistochemical staining for spirochetes.

Specimen Type	Microorganism	Microorganism Species	Culture and/or PCR Results	Special Stains*	Mycobacterial Immunohistochemistry
Lung	Bacteria (Acid-Fast)	*Nocardia*	Not performed	Twort+, GMS+, Fite+	Positive
Tonsil	Bacteria (Acid-Fast)	*Actinomyces*	Not performed	None performed	Positive
Stomach	Bacteria	*Helicobacter heilmanni*	Not performed	None performed	Negative
Stomach	Bacteria	*Helicobacter pylori*	Not performed	None performed	Negative
Soft tissue	Bacteria	N/A	Cultures grew *Escherichia coli* and *Tissierella praeacuta*	None performed	Negative
Rectum	Bacteria	*Treponema pallidum*	Not performed	None performed	Negative
Colon	Bacteria	Spirochetosis	Not performed	None performed	Negative
Colon	Bacteria	Spirochetosis	Not performed	None performed	Negative for spirochetes Positive for cocci bacteria
Stomach	Bacteria	*Helicobacter pylori*	Not performed	None performed	Negative for *H. pylori* Positive for other background bacteria
Larynx	Bacteria	N/A	Not performed	None performed	Positive
Skin	Bacteria	N/A	Not performed	None performed	Positive
Soft Tissue	Bacteria	N/A	Cultures grew MRSA	None performed	Positive
Skin	Bacteria	*Pseudomonas*	Cultures grew *Pseudomonas*	Fite-, GMS-, Twort equivocal	Positive
Skin	Bacteria	*Pseudomonas*	Cultures grew *Pseudomonas*	Twort+	Positive
Skin	Bacteria	*Pseudomonas*	Cultures grew *Pseudomonas*	Twort+	Positive

Vulva	Bacteria	N/A	Cultures grew VRE and *Pophyromonas*	Twort+	Positive (focal)
Soft Tissue	Bacteria	*Bartonella henslae*	Not performed	None performed	Negative
Soft tissue	Bacteria (*Mycobacteria*)	Atypical mycobacterium	Not performed	Twort+ (rods), Fite+	Positive
Skin	Bacteria (*Mycobacteria*)	Leprosy	Not performed	Fite+	Positive
GI Tract	Bacteria (*Mycobacteria*)	*Myocobacterium avium-intercellare (MAI)*	Not performed	ZN+	Positive
Larynx	Fungi	N/A	Not performed	None performed	Negative
Skin	Fungi	Dermatophytosis	Not performed	GMS+	Negative
Spleen	Fungi	*Histoplasmosis*	Not performed	GMS+	Negative
Toenail	Fungi	Onychomycosis	Not performed	GMS+	Negative
Skin	Fungi	Pityriasis versicolor	Not performed	None performed	Negative
Lung	Fungi	*Pneumocystis*	Not performed	GMS+, Fite-	Negative
Lung (Transplant)	Fungi	*Aspergillus*	Not performed	GMS+	Negative
Lung	Fungi	*Aspergillus*	Not performed	None performed	Negative
Skin	Fungi	*Candida*	Not performed	None performed	Negative for *Candida* Positive for background cocci bacteria
Esophagus	Fungi	*Candida*	Not performed	None performed	Negative for *Candida* Positive for background cocci bacteria
Esophagus	Fungi	*Candida*	Not performed	None performed	Negative for *Candida* Positive for background cocci bacteria
Lung	Fungi	*Blastomycosis*	Not performed	GMS+, Fite-	Positive (capsule)
Skin	Fungi	Chromoblastomycosis	Not performed	GMS+	Positive (capsule)
Lung	Fungi	*Coccidioidomycosis*	Not performed	GMS+	Positive (capsule)
Skin	Parasite	*Leishmania*	PCR was positive for *Leishmania*	GMS-, Fite-, Spirochete-	Positive

Figure 1 - 514

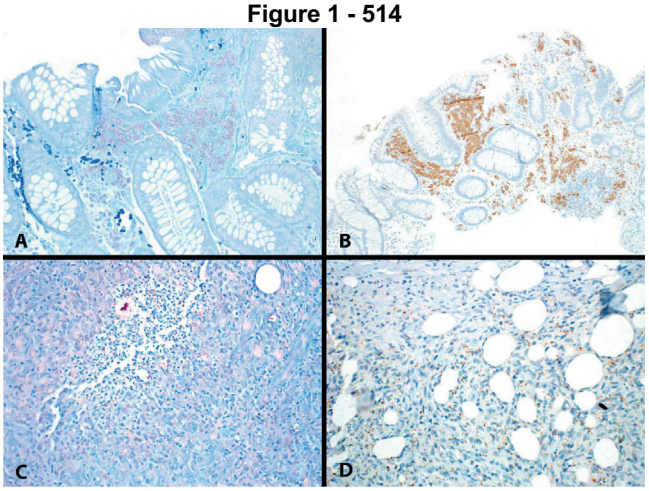

Figure 1. High-power magnification photomicrographs showing *Mycobacterium avium-intracellare* staining pattern with Ziehl Neelsen (**A**) and mycobacterial immunohistochemical (mIHC) stain (**B**) stains and atypical mycobacterium staining pattern with Fite acid fast stain (**C**) and with mIHC (**D**).

Figure 2 - 514

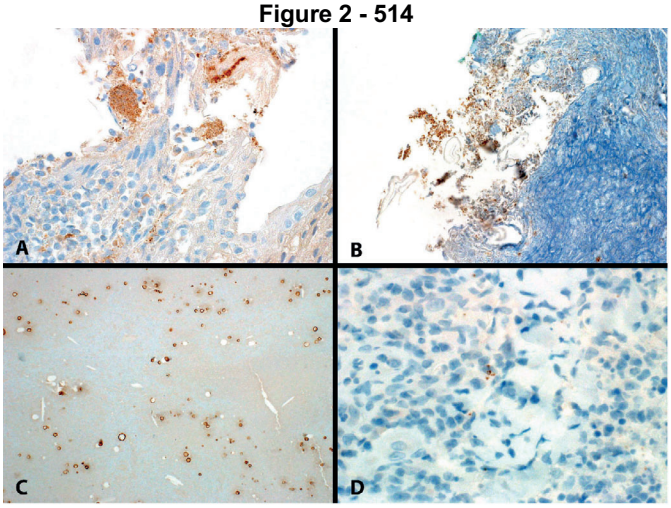

Figure 2. High-power magnification photomicrographs showing other microorganisms that stained positively with the mycobacterial immunohistochemical stain, including *Actinomyces* (**A**), *Pseudomonas* (**B**), *Coccidioides* (**C**), and *Leishmania* (**D**).

Conclusions: This is the first study to examine cross reactivity of the antimycobacteria antibody with various types of pathogens. Although it is highly sensitive for mycobacteria, it shows significant cross reactivity with other organisms, including encapsulated fungi and many other types of bacteria. The Biocare antibody is a sensitive but nonspecific stain that can be used as an alternative confirmation method for mycobacteria, but attention should be paid to inflammatory reaction and organism morphology when mIHC is positive, in order to avoid misdiagnosis.

515 Inter-Observer Agreement and Performance of a New Grading System for Invasive Pulmonary Adenocarcinoma

Wencheng Li[1], Omer Hassan[1], Mary Green[1], Alexandra Balmaceda[2], Emily Teague[1], Rebecca Steele[2]
[1]Wake Forest Baptist Medical Center, Winston-Salem, NC, [2]Wake Forest Baptist Health, Winston-Salem, NC

Disclosures: Wencheng Li: None; Omer Hassan: None; Mary Green: None; Alexandra Balmaceda: None; Emily Teague: None; Rebecca Steele: None

Background: The International Association for the Study of Lung Cancer (IASLC) pathology committee has recently established a grading system for resected invasive pulmonary adenocarcinoma. While the original study has shown it is practical and prognostically relevant, the reproducibility and performance have not been widely tested.

Design: Resected pulmonary adenocarcinoma between 2008 to 2015 was retrospectively identified and reviewed. Cases with at least five-year follow up were included and prognostic parameters including disease-free survival (DFS) and overall survival (OS) were collected. The inclusive cases were graded according to the IASLC system. The inter-observer agreement of the new system was compared with the original tumor grading, mitotic and nuclear grades. The survival curves were plotted using Kaplan-Merier curve and the difference between grades in DFS and OS was determined using log-rank tests.

Results: We identified 201 lung adenocarcinomas with surgical resection and adequate follow up. The original tumor grade was based on 2015 WHO classification of pulmonary adenocarcinoma (predominant patten-based). Nuclear and mitotic grades (from grade 1 to 3) were based on previously published criteria. The new grading system was based on the combination of predominant and high-grade patterns. Five graders including two pathology residents, one surgical pathology fellow and two practicing pathologists were involved in the reproducibility study. The overall agreement of the new grading system was 85.3% leading to a *k* value of 0.75 (95% confidence interval: 0.65-0.85) by Fleiss' *k* statistic. Most of the disagreements were recorded between grades 1 and 2. The agreement of the original grading system, mitotic grade and nuclear grade was 70.8%, 71.0% and 67.9% respectively, leading to the *k* value of 0.62, 0.56 and 0.45. A preliminary analysis of the predictive performance indicated that higher grade was associated with reduced DFS (p=0.009) and OS (p=0.01). More complete analysis including incorporation with tumor stage and other prognostic features as well as comparison with the original system are our next steps to further evaluate the performance of the new system.

Conclusions: We found substantial inter-observer agreement of the new grading system for lung adenocarcinoma, indicating this is a practical system for quick implementation in routine pathology practice. More importantly, our preliminary survival analysis showed its strong prognostic performance.

516 Genomic Landscape of Tumors with SMARCA4 Alterations in Lung and Other Solid Tumor Types

Hany Meawad[1], Parastou Tizro[2], Leonidas Arvanitis[1], Michelle Afkhami[1], Javier Arias-Stella[1]
[1]City of Hope National Medical Center, Duarte, CA, [2]City of Hope Cancer Center, Duarte, CA

Disclosures: Hany Meawad: None; Parastou Tizro: None; Leonidas Arvanitis: None; Michelle Afkhami: None; Javier Arias-Stella: None

Background: *SMARCA4* mutations have been identified in small cell carcinoma of ovary hypercalcemic type, SMARCA4-deficient thoracic sarcomas, and SMARCA4-deficient NSCLC. Some of these tumors have increased genomic instability, frequent *TP53* mutations, and higher tumor mutation burden. Although *SMARCA4* mutations are reported in subsets of poorly differentiated/undifferentiated tumors, data is still very limited. The goal was to assess the genomic landscape of tumors with *SMARCA4* alterations across all solid tumor types and their outcome.

Design: This was a retrospective study to evaluate all solid tumor cases with *SMARCA4* mutation identified by our 161 gene next generation sequencing (NGS) panel tested from 12/2017 through 09/2021. DNA and RNA were extracted from FFPE samples to perform NGS by Ion AmpliSeqTM technology and analyzed with the Ion Reporter and NextGENe software, design to detect for mutations, copy number variations and fusions. Microsatellite instability (MSI) was also evaluated by PCR. Tumor mutation burden (TMB) was analyzed starting January 2020. PD-L1 protein expression by immunohistochemistry was performed and calculated based on tumor type and clone utilized (PD-L1 223C FDA, KEYTRUDA). Clinical and pathologic information was retrieved from the electronic medical records.

Results: A total of 41/2580 (1.6%) sequenced cases had *SMARCA4* mutations. The mean patient age at diagnosis was 65 (range 41-89) years. Male to female ratio of 1:1. Primary tumor sites included lung (16/41; 39%), colon (3/41), liver (3/41), and other extra-pulmonary sites. Tumor types included adenocarcinoma, squamous cell carcinomas, melanoma. Lymph node or distant metastasis was present at time of diagnosis in 21/41 (51%). 13/41 (32%) patients had recurrence at a median of 10.3 months (range 2-32), and 16/41 (39%) died of disease at 13 months (range 1-35). MSI stable 27/28 (96%). TMB was high in 6/7 (86%). The most common co-occurring mutations included TP53 (25/41,61%), moreover cases with lung cancers have higher incidence of ERBB2 mutations 3/14 (21%) and K-RAS mutation 3/14 (21%). PD-L1 expression was present in 16/35 (46%).

Conclusions: Although *SMARCA4* alterations were mostly identified in lung carcinomas, other tumor sites included colon, ovaries and liver. Tumors with *SMARCA4* often had an advanced disease at time of presentation, and higher incidence of TP53 mutations with a possible role for immunotherapy.

517 Eligibility for Immunotherapy Based on TruSight Oncology 500 Molecular Testing

Josh Mo[1], Inji Baek[2], Evan Fernandez[3], Joel Oakley[2], Gloria Cheang[4], Rhonda Yantiss[3], Wei Song[5], James Solomon[1]
[1]New York-Presbyterian/Weill Cornell Medical Center, New York, NY, [2]Weill Cornell Medical College, New York City, NY, [3]Weill Cornell Medicine, New York, NY, [4]Weill Cornell Medical College, New York, NY, [5]Guardant Health, Red Wood City, CA

Disclosures: Josh Mo: None; Inji Baek: None; Evan Fernandez: None; Joel Oakley: None; Gloria Cheang: None; Rhonda Yantiss: None; Wei Song: *Speaker*, Lilly Oncology; *Speaker*, Bayer; James Solomon: None

Background: Immuno-oncology (IO) therapy has revolutionized cancer treatment, and it is FDA-approved for a wide variety of tumor types. Eligibility criteria include mismatch repair (MMR) protein deficiency as evaluated by immunohistochemistry (IHC), microsatellite instability (MSI) phenotype as determined by molecular testing, and elevated tumor mutation burden (TMB) defined as greater than 10 mutations per megabase (mut/Mb). While IHC remains the mainstay of MMR status determination, next generation sequencing platforms now allow for evaluation of MSI and TMB concurrently with comprehensive molecular profiling.

Design: MMR IHC was correlated with MSI and TMB status as determined by the TruSight Oncology 500 Assay (TSO500, Illumina, San Diego) in a cohort of 40 cases. TSO500 uses hybridization-capture based chemistry, and libraries were sequenced on the NextSeq 550Dx system. The cohort included 23 cases that were part of the assay validation and 17 cases of gastrointestinal (GI) tumors that were performed clinically. Tumor types included colorectal (n=24), endometrial (n=9), upper GI (n=3), cholangiocarcinoma (n=2), pancreatic (n=1), and appendiceal (n=1). MSI was classified as follows: High if >20% of microsatellites were unstable, equivocal for 10-20%, and stable for <10%. TMB was calculated from tumor-only sequencing data by the Illumina software and classified as high if >10 mut/Mb.

Results: The concordance of MSI, MMR and TMB is shown in **Table 1.** Notably, the three MSI-equivocal cases were all endometrioid adenocarcinoma. All MSI-high and equivocal cases exhibited high TMB (median 37.4, range 12.8-83.0). Reproducibility testing was performed for MSI (intra-assay standard deviation (SD) = 1.46%; inter-assay SD = 2.13%) and TMB (intra-assay SD = 0.70; inter-assay SD = 1.14). We next examined a subset of 17 GI cases that were MMR preserved by IHC. All were MSS. One of 17 cases demonstrated a TMB of 13.1 mut/Mb, qualifying the patient for immuno-oncology therapy. In three cases, the 95% confidence interval of TMB spanned the TMB-H threshold of 10 mut/Mb (9.6, 9.4, and 9.4 mut/Mb, respectively).

	TSO500 Result		
Immunohistochemistry Result	**MSI-high (>20% sites)**	**MSI-equivocal (10-20% sites)**	**MSS (<10% sites)**
MMR Loss	10	3	0
MMR Retained	0	0	27
Tumor Mutation Burden (mut/Mb)	**MSI-high (>20% sites)**	**MSI-equivocal (10-20% sites)**	**MSS (<10% sites)**
TMB-High (>=10)	10	3	3
TMB-Low (<10)	0	0	24*

*3 cases were close to the TMB threshold (9.6, 9.4, and 9.4 mut/Mb, respectively).

Conclusions: Multiple criteria determine eligibility for IO therapy, and it is important to recognize advantages and limitations of various testing modalities. In patients with advanced-stage MMR-retained GI tumors, there is clinical utility for TMB determination. However, this study also highlights the need for clinical trials to correlate IO response with accurate TMB cutoffs based on tumor type.

518 Exploring Potential Innate Immune Targets to Treat Fibrosis and Chronic Inflammation in Chronic Graft-Versus-Host Disease

Nathan Paulson[1], Cristabelle De Souza[2], Lu Cui[2], Tristan Lerbs[2], Jessica Poyser[2], Maryam Kooshesh[3], Atif Saleem[2], Kerri Rieger[4], Ryanne Brown[4], Bernice Kwong[2], Sebastian Fernandez-Pol[5], Sally Arai[2], Judith Shizuru[5], Antonia Mueller[6], Gerlinde Wernig[7]
[1]Stanford Health Care, Stanford, CA, [2]Stanford University, Stanford, CA, [3]Mount Sinai Hospital, New York, NY, [4]Stanford Medicine/Stanford University, Stanford, CA, [5]Stanford University Medical Center, Stanford, CA, [6]University Hospital Zurich, Zurich, Switzerland, [7]Stanford University School of Medicine, Stanford, CA

Disclosures: Nathan Paulson: None; Cristabelle De Souza: None; Lu Cui: None; Tristan Lerbs: None; Jessica Poyser: None; Maryam Kooshesh: None; Atif Saleem: None; Kerri Rieger: *Consultant*, Pfizer; *Advisory Board Member*, Kyowa Kirin; Ryanne Brown: None; Bernice Kwong: None; Sebastian Fernandez-Pol: None; Sally Arai: None; Judith Shizuru: None; Antonia Mueller: None; Gerlinde Wernig: None

Background: Chronic graft-vs-host-disease (GVHD) is a major complication of allogeneic hematopoietic stem cell transplant and is characterized by an immune response resulting in chronic inflammation and eventual tissue fibrosis. Sclerodermatous GVHD is a severe form of skin-predominant chronic GVHD which manifests as marked skin and subcutaneous fibrosis and has a particularly poor prognosis and response to current therapies. Current understanding of the pathogenesis of fibrosis in these cases is extremely limited. JUN is a subunit of AP-1, a transcription factor involved in the regulation of gene expression in the acute phase response, which has recently been implicated in the pathogenesis of other fibrotic diseases. CD47 is an anti-phagocytic immune checkpoint protein which is known to be a key driver of impaired cell removal in malignancy and inflammatory responses. We hypothesized that the dermal fibroblasts present in sclerodermatous GVHD would show increased expression of JUN, CD47, and other important regulators of the immune response in GVHD in comparison to control samples, which has implications for the molecular pathogenesis of fibrosis in this disease and potential therapeutic targets.

Design: After IRB approval, a tissue microarray was created using skin biopsies from 45 patients with sclerodermatous GVHD and subsequently stained with SMA, Vimentin, JUN, CD47, IL-6, PDL-1, and PDGFRA. All samples were taken from patients with skin score 3 chronic GVHD by NIH criteria. Negative control tissue from normal human skin was also stained. For each case, presence and intensity of staining of all antibodies were calculated for all fibroblasts.

Results: Tissue microarray analysis and immunofluorescence staining revealed strong expression and activation of JUN in the dermal fibroblasts of the sclerodermatous GVHD patient cohort relative to healthy skin tissue controls (60% vs. 15%, $p < .0001$). Dermal fibroblasts in the cohort were also positive for collagen and showed increased expression and intensity of CD47, PDL-1, IL-6, and PDGFRA in a subset of patient samples.

Conclusions: We show that dermal fibroblasts present in chronic GVHD show increased expression and intensity of JUN, CD47, and other important regulators of the immune response. This is a novel finding in this disease and suggests important underlying factors in its pathogenesis.

519 The European Organisation for Research and Treatment of Cancer (EORTC) Protocol for Sentinel Lymph Node Biopsy (SLNB) Reveals a High Number of Nodal Nevi and a Strong Association With Nevus-associated Melanoma

Costantino Ricci[1], Emi Dika[1], Martina Lambertini[1], Francesca Ambrosi[2], Federico Chiarucci[3], Stefano Chillotti[1], Michelangelo Fiorentino[2], Erich Fabbri[4], Daniela Tassone[5], Giulia Veronesi[5], Federico Tartari[3], Barbara Corti[1]
[1]S.Orsola-Malpighi Hospital, University of Bologna, Bologna, Italy, [2]Maggiore Hospital, University of Bologna, Bologna, Italy, [3]Alma Mater Studiorum-University of Bologna, Bologna, Italy, [4]Ospedale maggiore Bologna, Bologna, Italy, [5]My Institution Is Not Listed, Bologna, Italy

Disclosures: Costantino Ricci: None; Emi Dika: None; Martina Lambertini: None; Francesca Ambrosi: None; Federico Chiarucci: None; Stefano Chillotti: None; Michelangelo Fiorentino: None; Erich Fabbri: None; Daniela Tassone: None; Giulia Veronesi: None; Federico Tartari: None; Barbara Corti: None

Background: The diagnosis of nodal nevi (NN) is challenging as they mimic melanoma metastases (MM), especially if found in lymph nodes (LNs) evaluated for staging purposes of melanoma. The incidence of NN ranges between 1%-11%, due to the nature of the primary tumor, the analyzed specimens and the protocols adopted for the pathological evaluation. Herein, we assessed the

incidence of NN and the association with the clinical-pathological features of primary melanoma, adopting the updated European Organisation for Research and Treatment of Cancer (EORTC) protocol for sentinel lymph node biopsy (SLNB).

Design: All cases of paired melanoma and SLNBs were retrospectively evaluated (April 2019-May 2020). Melanoma and SLNBs had been sampled, diagnosed and staged according to the updated EORTC protocol for SLNB, the 2018 WHO Classification of Skin Tumor, the 2020 CAP protocol for melanoma reporting and the 8th edition of the AJCC. The correlation between NN and clinical-pathological features of the primary melanoma were investigated with appropriate tests [χ^2 test for dichotomous and categorical data; Kruskal-Wallis (normal distribution) and one-way ANOVA (non-normal distribution) for continuous data]; the variables which resulted significant (*p-value* < *0.05*) were included in the forward logistic regression model (multivariable analysis).

Results: 81 patients and a total of 186 lymph nodes (LNs) were included. Eleven patients had only NN and 4 had both NN and MM (18.5%); 29 LNs (15.6%) showed at least one NN and 12 (6.5 %) showed more than one NN (a total amount of 43 NN was detected). All NN and none MM stained for p16. NN were associated with age < 60 years (*p: 0.042*), no ulceration (*p: 0.025*) and nevus-associated melanoma (NAM) (p: 0.018), with this latter being the only predictor at the logistic regression model (*p: 0.022*).

#chi-square test;
*Kruskal-Wallis test;
°one-way ANOVA test;
forward logistic regression model;

M: male; F: female; NAM: nevus-associated melanoma; LNs: lymph nodes; NN: nodal nevi; MM: melanoma metastasis; n: number of patients for which clinical-pathological features were present and/or evaluated; (%): percentage compared to the specific analyzed group (Study population, *Group 0* and *Group 1*); *Group 0*: absence of NN; *Group 1*: presence of NN regardless of synchronous MM; mm^2: square millimeter; in each column we reported the total number of patients (*Study population:* 81, *Group 0:* 66 and *Group 1:* 15).

Table 1. Summary of the main clinical-pathological features of the case series and their distributions among *Group 0* and *1* (chi-square, Kruskal-Wallis, one-way ANOVA tests and forward logistic regression model).

Sex		46 (56.8%) M; (43.2%) F		
Age, mean value and range (years)		59.2; 24-86		
Age ≥ 60 years		46 (56.8%)		
Site				
Head and neck		4 (4.9%)		
Upper extremities		13 (16%)		
Lower extremities		16 (19.8%)		
Dorsum and trunk		48 (59.3%)		
Ulceration of melanoma		25 (30.9%)		
NAM		15 (18.5%)		
Breslow thickness, mean value and range (mm)		2.2; 0.8-8		
pT stage				
pT1b		29 (35.8%)		
pT2a		18 (22.2%)		
pT2b		3 (3.7%)		
pT3a		7 (8.6%)		
pT3b		9 (11.1%)		
pT4a		2 (2.5%)		
pT4b		13 (16 %)		
Molecular data				
WT		3 (13.6%)		
BRAF		14 (63.6%)		
NRAS		5 (22.8%)		
MM				
Patients positive for MM		24 (29.6%)		
LNs positive for MM		31 (16.6%)		
Total number of MM		32		
MM site		11 (sub-capsular), 10 (parenchymal),		
		2 (combined), 1 (extensive multifocal)		
Dimension of MM, range (mm)		0.80-1.60		
Extracapsular extension		8 (9.9%), 4 focal and 4 diffuse		
NN				
Patients positive for NN		15		

LNs positive for NN		29 (15.6%)		
Total number of MM		43		
NN site		8 (capsular), 1 (sinusoidal),		
		1 (extra-capsular), 5 (mixed)		
Dimension of NN, range (mm)		0.1-1.00		
NN morphology		14 (nevocytic), 1 (blue-like)		
	Study population, n (%)	**Group 0, n (%)**	**Group 1, n (%)**	***p-value***
Age ≥ 60 years	46/81 (56.8)	41/66 (62.1)	5/15 (33.3)	*0.042#*
Male sex	46/81 (56.8)	37/66 (56)	9/15 (60)	*0.781#*
Lower extremities	16/81 (19.8)	15/66 (22.7)	1/15 (6.7)	*0.158#*
Vertical growth phase	74/81 (91.4)	61/66 (92.42)	13/15 (86.7)	*0.474#*
Angioinvasion	38/81 (58.5)	25/66 (37.9)	13/15 (86.7)	*0.051#*
Perineural infiltration	6/81 (7.4)	5/66 (7.6)	1/15 (6.7)	*0.903#*
Ulceration	25/81 (30.9)	24/66 (36.4)	1/15 (6.7)	*0.025#*
Mitosis>1/mm2	57/81 (70.4)	49/66 (74.2)	8/15 (53.3)	*0.109#*
NAM	15/81 (18.5)	9/66 (13.6)	6/15 (40)	*0.018#*
Breslow Thickness, mean value (mm)	81/81 (100)	0.92	0.87	*0.124**
Age, mean value (years)	81/81 (100)	61.5	49.4	*0.009°*
Age ≥ 60 years				*0.339*
Ulceration				*0.094*
NAM				*0.022*

Figure 1 - 519

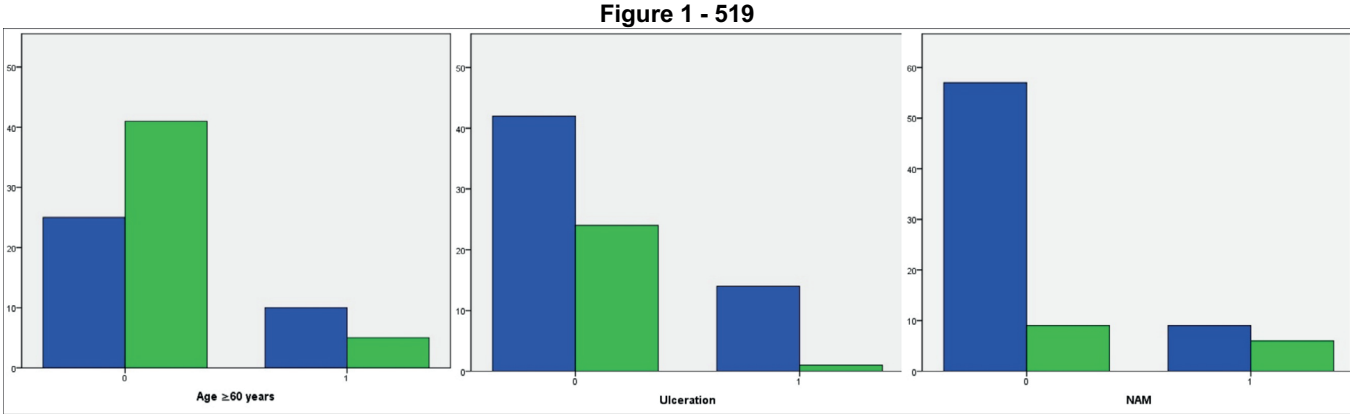

Conclusions: The updated EORTC protocol shows a higher number of NN compared to previous studies, expanding the amount of data regarding the association between NN and specific clinical-pathological features of primary melanoma (NAM, onset age and ulceration). Besides, we found that the appropriate application of the commonly available stains (H&E, p16 and HMB45) is sufficient to allow a correct diagnosis with this protocol and rule out a dangerous over-diagnosis of melanoma metastases.

520 An Assessment of Racial and Gender Disparities in Genetic Counseling or Testing for Patients with Mismatch Repair Deficient Tumors

Jennifer Vazzano[1], Jewel Tomlinson[1], Peter Stanich[1], Rachel Pearlman[1], Wei Chen[1], Heather Hampel[1], Wendy Frankel[1]
[1]The Ohio State University Wexner Medical Center, Columbus, OH

Disclosures: Jennifer Vazzano: None; Jewel Tomlinson: None; Peter Stanich: *Grant or Research Support*, Pfizer Inc, PTEN Research Foundation, Freenome, Jannsen Pharma, Emtora Biosciences; Rachel Pearlman: None; Wei Chen: None; Heather Hampel: *Advisory Board Member*, Promega, Invitae Genetics, Genome Medical; *Consultant*, GI OnDemand; Wendy Frankel: None

Background: Patients with absence of a mismatch repair protein(s) on immunohistochemistry (IHC) found by universal tumor screening (UTS) are considered to have mismatch repair deficiency (dMMR). Those with absence of MLH1 and PMS2 need follow-up testing for acquired *MLH1* hypermethylation (MHM), which is done directly or indirectly by assessing for *BRAF* mutation. Patients with dMMR tumors with MHM ruled out when indicated should undergo genetic counseling and testing to determine if they have Lynch syndrome (LS). Gender and racial disparities have been seen in multiple health care settings including follow-up genetic counseling and testing in UTS programs. Our goal was to see if there were gender, racial or ethnic disparities in follow-up genetic counseling and testing at a tertiary care institution.

Design: Electronic medical records were reviewed for all cases (colorectal, endometrial, others) screened with UTS between 1/9/2009 and 5/27/2021 to note patient gender, race, ethnicity; results for MMR IHC, *BRAF* mutation or MHM; and appointments with genetics and uptake of genetic testing.

Results: 3145 patients were diagnosed and got UTS with MMR IHC including 1538 males and 1607 females. 2718 were white, 295 black, 51 Asian, and 33 Hispanic. Race was not available for 48. Among 3145 cases, 205 (6.5 %) had a non-methylated dMMR tumor, without a *BRAF* mutation or MHM (when indicated), and had a clear indication for genetic counseling. There were 113 males (55.1%) and 92 females (44.9%). Of the 202 with known race, 168 were white (83.2%), 23 black (11.4%), 10 Asian (5.0%), and 1 was Hispanic (0.5%). Of 205 dMMR patients, 96 (46.8%) were seen by genetics; rates were similar for men (44.2%) and women (50%). By a chi-squared test of independence, we did not find any significant differences in patients seen by genetics according to race or ethnicity with 47.0% (79/168) white, 39.1 % (9/23) black, 70% (7/10) Asian and 100% (1/1) Hispanic (p=0.28). Notably, 100% of patients seen by genetics elected to pursue genetic testing.

	White	Black	Asian	Hispanic	Male	Female
Total	2718	295	51	33	1538	1607
*** Genetics indicated**	168/2718 (6.2%)	23/295 (7.8%)	10/51 (19.6%)	1/33 (3.0%)	113/1538 (7.3%)	92/1607 (5.7%)
Patients seen by genetics	79/168 (47.0%)	9/23 (39.1%)	7/10 (70.0%)	1/1 (100.0%)	50/113 (44.2%)	46/92 (50.0%)
Genetic Testing Uptake	79 (100%)	9 (100%)	7 (100%)	1 (100%)	50 (100%)	46 (100%)

***Genetics indicated =dMMR by IHC and no *MLH1* methylation or *BRAF* mutation when indicated.**

Conclusions: While the overall rate of genetic counseling completion for patients with non-methylated dMMR tumors (46.8%) needs improvement, no significant disparities were seen by gender or race. Rates in black and white patients and males and females were similar. Higher rates were seen in Asian and Hispanic patients but were not statistically significant. Importantly, when seen by genetics patients were equally likely to pursue germline genetic testing, regardless of race or gender.

521 Revisiting the Use of CK7 and CK20 Immunohistochemical Stains in Pathological Diagnoses

Bangchen Wang[1], Jiaoti Huang[2]
[1]Duke University Medical Center, Durham, NC, [2]Duke University, Durham, NC

Disclosures: Bangchen Wang: None; Jiaoti Huang: *Consultant*, Kingmed; *Advisory Board Member*, MoreHealth; *Advisory Board Member*, OptraScan; *Advisory Board Member*, Genetron; *Consultant*, Omnitura; *Consultant*, Vetonco; *Stock Ownership*, York Biotechnology; *Consultant*, Genecode; *Consultant*, VIVA Biotech; *Stock Ownership*, Sisu Pharma

Background: Immunohistochemical (IHC) stains for cytokeratin-7 (CK7) and cytokeratin-20 (CK20), especially their combination, are among the most commonly used markers to help determine the tumor site of origin. However, as newer biomarkers of better sensitivity and specificity become increasingly available, it is timely to examine the true value of CK7/CK20 coordinate expression in different clinical settings. In this study, we retrospectively reviewed 600 cases for which CK7 and/or CK20 IHC stains were performed and evaluated their contribution to the final diagnosis.

Design: From year 2016 to 2020, IHC stains for CK7 and/or CK20 were performed on 4421 surgical pathology cases in our institution (1689 CK7-only, 516 CK20-only, and 2216 CK7-and-CK20 cases). We randomly selected 600 cases and retrospectively reviewed the results of CK7, CK20 and all other IHC stains. For each case, the level of contribution of the CK7/CK20 stains to the final diagnosis was scored as one of the three categories: “none”, “minor” or “major” (Figure 1).

Results: As shown in Figure 2A, in cases where both CK7 and CK20 stains were performed, the staining results had major contribution in only 5% of the cases. In cases where only CK7 or CK20 stain was performed, the percentage of cases with major contribution is increased to 34% and 69% respectively. Detailed analysis demonstrates that CK7 and CK20 stains, used singly, are most useful in the diagnosis of a limited number of pathologic entities with distinct CK7 or CK20 expression patterns, such as Paget’s diseases, kidney tumors, flat urothelial lesions, and Merkel cell carcinoma. In cases where both CK7 and CK20 stains were performed, 233 of 261 cases had a specific or suggestive diagnosis clinically and/or histologically. As shown in Figure 2B, in 111 of the 233 cases, the pattern of CK7/CK20 coordinate expression was inconsistent with the final diagnosis; of these cases, other IHC markers contributed to the final diagnosis 92% of the time. Conversely, in cases where other IHC markers were not helpful (29 of 233 cases), CK7/CK20 contributed to the final diagnosis only 34% of the time.

Figure 1 - 521

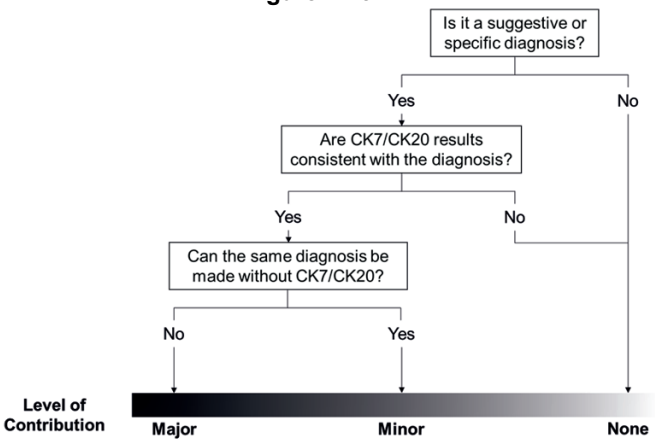

Figure 1. The algorithm used to score the level of contribution of CK7 and/or CK20 stains.

Figure 2 - 521

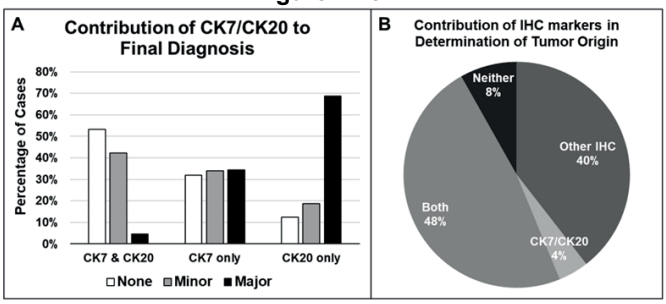

Figure 2. A. Percentage of cases where CK7 and/or CK20 had no, minor, or major contribution to the final diagnosis among the three groups (CK7&CK20 = cases where both CK7 and CK20 stains were performed; CK7 only = cases where CK7 but not CK20 stains were performed; CK20 only = cases where CK20 but not CK7 stains were performed). **B.** Contribution of CK7/CK20 coordinate expression and other IHC markers to determination of tumor origin in cases where both CK7 and CK20 stains were performed. "CK7/CK20" = only CK7/CK20 contributed; "Other IHC" = only IHC markers other than CK7/CK20 contributed; "Both" = both contributed; "Neither" = neither contributed.

Conclusions: In conclusion, our results suggest that the coordinate expression of CK7 and CK20 is generally not helpful in arriving at the final diagnosis when more sensitive and specific IHC markers are available. Reducing the use of CK7/CK20 IHC stains may significantly reduce unnecessary cost to healthcare, and help optimize pathology practice in the era of value-based care.